FINITE ELEMENT MODELING OF THE EFFECT OF CREEP DAMAGE ON A MAGNETIC DETECTOR SIGNAL FOR SEAM-WELDED STEEL PIPES

M.J. Sablik
Southwest Research Institute
P.O. Drawer 28510
San Antonio, Tx 78228-0510

D.C. Jiles
Center for NDE
Iowa State University
Ames, IA 50011

M.R. Govindaraju
Magnetica, Inc.
P.O. Box 1521
Ames, IA 50014

INTRODUCTION

Creep damage is the result of slow plastic flow of metal under stress and at high temperature, typically about 50% of the absolute melting temperature. If there is enough creep damage, the end result can be sudden, catastrophic failure. Lately, creep has become a serious problem in the petrochemical industry and in fossil fuel power plants, where alloy steel pipes are subjected to stress and high temperature for long periods of time.

The problem is particularly acute in seam-welded pipe because the creep damage develops first inside the pipe wall and doesn't appear at the wall surface until the pipe is almost ready to fail. Thus, it is possible to have failure almost without warning.

This dangerous situation can occur with seam-welded pipe because the cross-section of the weld is shaped like two trapezoids with the larger bases of the trapezoids on the inside and outside wall of the pipe and with the smaller trapezoid bases meeting in the interior to form an interior cusp. The stress concentrates at the cusp, and it is at the cusp where creep damage begins. The creep damage then works its way toward the inside and outside pipe surfaces. [1] A standard technique for detecting creep damage is replication [2], which involves making a wax or epoxy replica of the pipe surface and subsequent microscopic analysis. For seam welds, another detection method is required because creep damage is not at the surface.

Since the pipe is ferromagnetic steel, magnetic techniques would seem to be a promising way to detect creep damage. Microstructural changes due to creep should

Review of Progress in Quantitative Nondestructive Evaluation, Vol. 17
Edited by D.O. Thompson and D.E. Chimenti,, Plenum Press, New York, 1998

produce changes in domain wall pinning, in turn producing changes in magnetic properties. These magnetic changes should be detectable with rather simple instrumentation.

Such considerations have led to research on magnetic changes due to creep damage. Experimental research has demonstrated that creep damage results generally in a reduction of magnetic properties, so that properties such as coercivity, remanence, permeability, and hysteresis loss all decrease as a result of creep damage. [3,4] A mathematical hysteresis model, which models the magnetic effects of creep damage, has been used to explain the experimental observations. [3,4]

A finite element model, investigating the magnetic effects of a nonuniform creep damage distribution about the cusp of a seam weld, has been additionally employed to predict the effect of the creep damage on the secondary emf detected by a magnetic C-core detector. [4,5] Although the simulation suggested that a detectable emf reduction would be obtained when creep damage existed, the simulation had a major defect in that it assumed that weld material, HAZ (heat-affected-zone) and base metal all had the same coercivity, remanence, hysteresis loss, and permeability behavior (i.e. that they all had the same initial magnetization curve), and this is in general not the case.

It is necessary to know the magnetic changes due to the weld alone before one can determine how much of the total magnetic effect is due to creep damage. The purpose of this paper is to include in a finite element simulation, the magnetic changes due to the weld and HAZ prior to creep and then to compute the magnetic changes due to the creep damage on top of that.

PHYSICAL MODEL FOR MAGNETIC CHANGES DUE TO CREEP DAMAGE

During creep, microstructures such as voids and dislocation densities in the grains and cavitation and microcracks at the grain boundaries, undergo continuous change. In the initial stages of creep, metallographic studies reveal that voids, impurity atoms, and dislocations accumulate on the grain boundary to form grain boundary cavitation. As cavities on the grain boundary get larger and coalesce, microcracks start forming. In the final stages of creep, the microcracks join up, becoming larger cracks, which can result ultimately in failure.

Magnetically, these microstructural changes have two significant effects. As voids, impurities, and dislocations move out of the matrix, the pinning sites in the grain are decreased and a lower magnetic coercivity results. A second effect is that grain boundary cavitation produces a demagnetization field. This demagnetization field opposes the applied field, reducing net flux density, and producing a reduction in such quantities as remanence and permeability. Reduction in both coercivity and remanence results in reduced hysteresis loss (i.e. reduced area inside the hysteresis loop.)

These magnetic changes can be placed into the magnetic hysteresis model.[6,7] First, magnetic poles formed at cavities produce a demagnetization field -DM, which opposes the applied field H, resulting in an effective field given by [3,4]

$$H_e = (H + \alpha M_a) - DM_a + (3\sigma/2\mu_o)(d\lambda/dM_a) \quad (1)$$

inside the material. The first two terms arise from the original Jiles-Atherton model.[6] H is the applied field, and αM_a is an effective field contribution due to interaction of domains. The anhysteretic magnetization M_a refers to the thermodynamic equilibrium magnetization, to which the magnetization of the system tends. The final term was incorporated by Sablik et al. [7,8] and introduces the effect of stress σ on the effective field as being dependent on the magnetization derivative of the magnetostriction λ, which is the length change due to magnetization. The third term describes the effect of the demagnetization field. The constant D is assumed to be proportional to the volume fraction of the material that is cavity, and is written as

$$D = k_1(V_c/V), \tag{2}$$

where V_c/V is volume fraction of cavities, and k_1 is a constant.

According to the model [6,7], the total magnetization can be written as

$$M = M_i + c(M_a - M_i), \tag{3}$$

where c is a constant obtainable from extrapolation to zero stress and field. [6] M_i is the irreversible component of magnetization associated with domain wall pinning and unpinning. The term in (3) proportional to c is due to domain wall bending, [6] and is expressed in terms of the difference between irreversible M_i and anhysteretic M_a. M_a is given by

$$M_a = M_s \mathcal{L}(H_e/a), \tag{4}$$

where M_s is the saturation magnetization, $\mathcal{L}(x)=\coth x - 1/x$, and a is a constant which is a property of the material. The irreversible magnetization M_i depends in a complicated way on M_a, and is determined self-consistently through the differential equation

$$\frac{dM_i}{dH} = \frac{M_a - M_i}{\frac{k^*\delta}{\mu_o} - \left[\alpha^* + \frac{3\sigma}{2\mu_o}\left(\frac{d^2\lambda}{dM_a^2}\right)\right](M_a - M_i)}, \tag{5}$$

where $\delta = \pm 1$, depending on whether H is increasing (+) or decreasing (-), and where $\alpha^* = \alpha - D$ and k^* is the effective domain wall pinning strength.

Effective pinning strength k^* is a measure of the average energy with which domain walls are pinned at pinning sites. Imposition of an applied H helps overcome pinning energy and domain walls break free until they are repinned elsewhere with even greater pinning energy. The pinning strength also determines the coercive field H_c, which is the field that is needed to reduce a magnetized material to zero magnetization. If the number of pinning sites inside the grains is reduced owing to creep, the pinning strength will be correspondingly reduced. Mathematically, this effect is expressed as

$$k^* = k(1 - k_2(V_c/V)), \tag{6}$$

which postulates that reduction in pinning strength correlates with cavity volume fraction, since cavities form concomitantly with the reduction in pinning sites. The constant k_2 is the creep pinning factor. The constant k is the original pinning strength, prior to creep damage.

Note that in the model, the parameters affected by creep are those that carry an asterisk, namely α^* and k^*. These both depend on volume fraction of cavitation. The irreversible magnetization depends explicitly on k^* and α^*, and also indirectly on α^* through its dependence on M_a. The total magnetization M is a linear combination of M_i and M_a, as given in (3). From M, the flux density B in the material can be obtained via $B=\mu_0(H+M)$.

APPLICATION TO A FINITE ELEMENT COMPUTATION FOR SEAM WELDS, TAKING WELD AND HAZ MAGNETIC PROPERTIES INTO ACCOUNT

The key ingredient of the finite element calculation is in the assignation of different initial magnetization curves for each element in the steel material. The magnetization curve for each element is computed depending on the amount of creep damage and stress present in the element. The total magnetic behavior results from the cumulative effect of all these different initial magnetization curves. Although stress could be introduced into the computation, the simulation was done for zero stress, since that corresponds to an unloaded pipe without steam in it (and NDE measurements would presumably be done on a unloaded pipe). The simulation package ANSYS was used because it had the capability of assigning different initial magnetization curves to individual elements.

Other assumptions in the computation are as follows:

1) Because the seam weld is very long in directions perpendicular to the width of a seam weld, only a *two-dimensional* simulation is needed.
2) A flat plate is assumed instead of a curved plate as a first approximation.
3) The magnetic C-core is assumed to rest flush against the specimen surface. This means that no leakage field arises due to any air space between the pole piece and the specimen.
4) The C-core is placed directly across the width of the seam weld.
5) Maximum creep damage at the seam weld cusp is set at $V_c/V=0.06$, and the amount of creep damage (V_c/V) in each element is diminished proportionally with distance from the cusp in a band of creep damage about the fusion line of the weld. The band of creep damage stops before the bottom and top surfaces of the specimen are reached.

These assumptions all were used in the prior simulation. [4,5]

A new assumption is that the intial magnetization curves utilized for each element take also into account the weld magnetic properties, differentiating between the properties of the weld material, the heat-affected zone, and the base metal. Data for such differentiation of magnetic properties does not exist for 2.25 Cr1Mo steel, which is the steel used in power plant steam pipes. However, data does exist showing the changes in magnetic properties from base metal to HAZ to weld metal for other types of steel. In particular, we use the data of Thompson et al [9], tabulated as found in Table I, for welds in various steels for the case of as-welded samples and for renormalized (reannealed) welds. It is seen that differences in permeability in the as-welded samples tend to be almost eliminated in renormalized samples. Thus, a worst case may be assumed for the as-welded samples, corresponding to $\mu_m/\mu_o = 1271$ for the base metal, $\mu_m/\mu_o = 784$ for the HAZ, and $\mu_m/\mu_o = 571$, where μ_m/μ_o is the maximum relative permeability assigned to the region in question. (Mathematically, such permeabilities were obtained (equivalently) by imposing a nonzero compressive stress on the base metal until the desired relative permeability was obtained. The corresponding initial magnetization curves were then stored as the initial magnetization

Table I. Different maximum relative permeabilities obtained for base metal (parent), HAZ, and weld material in different steels

for the as-welded samples			for renormalized welds		
$\mu_{max} \pm 80$			$\mu_{max} \pm 80$		
Parent	*HAZ*	*Weld*	*Parent*	*HAZ*	*Weld*
1288	889	848	831	803	877
931	752	491	849	939	906
1006	759	543	925	714	804
1054	731	595	1030	1033	938
1090	692	641	761	922	719

curves for HAZ and weld metal. In practice, if more complete magnetic measurements were available, the fitted curve would be obtained by fitting all the magnetic parameters available. [10]) Figure 1 shows the hysteresis and inital magnetization curves corresponding to the weld, HAZ and base metal regions, as used in the simulation.

Figure 2 shows the finite element assignment of area regions, with finer area discretization shown in the weld vicinity, and additional finer discretization in the weld cusp region. The three distinct regions - weld, HAZ, and base weld - are shown in different shadings. The C-core detector is shown with primary coil regions also shaded differently. Final mesh discretization of elements is established by the software. The band of creep damage along the weld fusion line is built into the calculation via the initial magnetization curves utilized for the individual element areas in the vicinity of the fusion line.

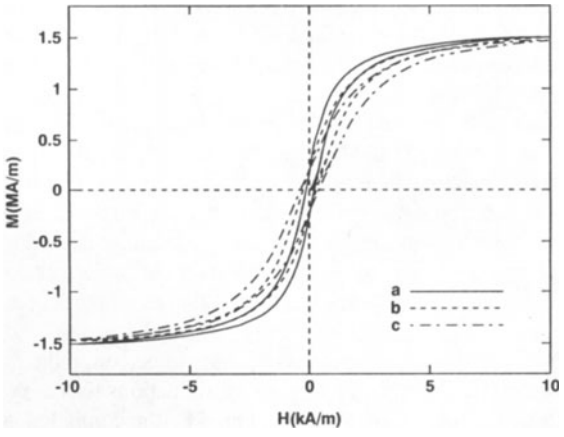

Figure 1 - Hysteresis and initial magnetization curves for (a) base metal (solid), (b) HAZ (dashed), and (c) weld metal (hashed).

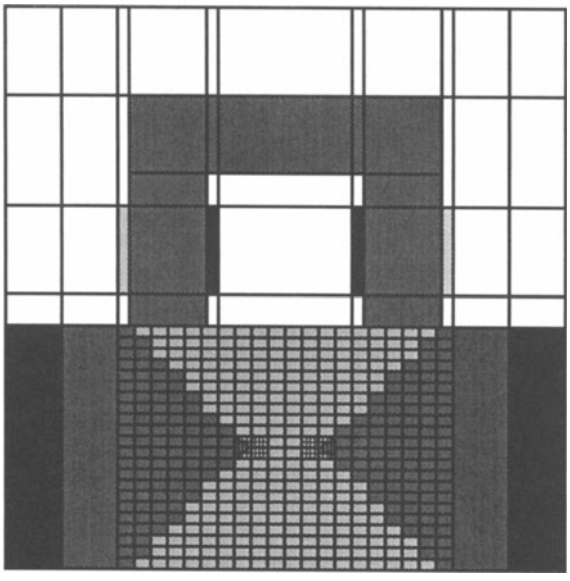

Figure 2 - ANSYS area discretization of a magnetic C-core detector above a seam weld region.

RESULTS

The simulation was performed for four cases:

1) specimen is base metal only;
2) Weld, HAZ, and base metal have different μ/μ_0, but no creep damage exists;
3) Weld, HAZ, and base metal have different μ/μ_0, *and* creep damage exists;
4) Weld, HAZ, and base metal have the *same* μ/μ_0 *and* creep damage exists.

The computed emf from case (1) is taken as a base value for the computed percent emf reduction for each of cases (2) and (3). Figure 3 shows percent reductions in emf for case (3) compared to the percent reduction for case (2). It is seen that the greater portion of the reduction in emf is due to the magnetic differences between weld regions, particularly for low primary currents. Nevertheless, an approximately 5% additional reduction is found due to the creep damage. This is feasible to detect, even over the background of the reduction due to weld region differences, which first has to be calibrated in practice.

An alternate way to do comparisons is to compute percent reductions for case (4) above compared to case (1), and to compute percent reductions for case (3) compared to case (2). The results for the former are shown in Fig. 4 by the computed ⊙ points. The results for the latter $((emf_3-emf_2)/emf_2)$, represented by the X points, are what would

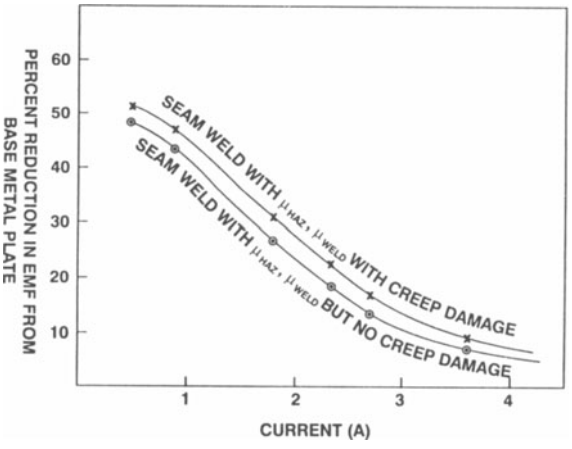

Figure 3 - Percent reductions in emf computed when magnetic differences between weld regions are considered for the case of (a) creep damage and (b) no creep damage.

actually be measured in an NDE measurement. Comparing ⊙ to X is equivalent to comparing our finite element results computed previously [4,5] to the results now predicted for an NDE measurement of creep damage. The major difference between the two computed results is that the peak in percent reduction at low primary currents is more diffuse when the magnetic differences between the various weld regions is taken into account.

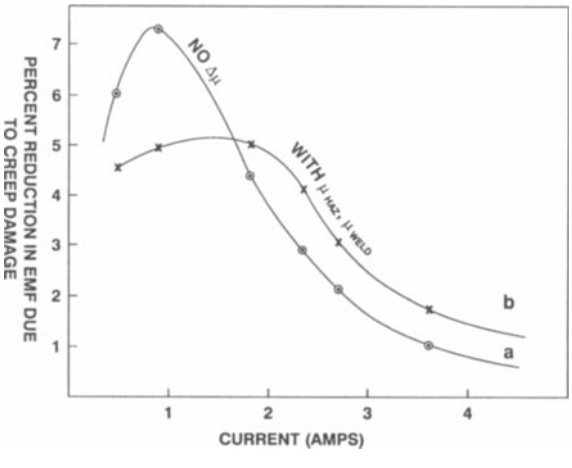

Figure 4 - Percent reductions only due to creep damage when magnetic differences between weld regions are (a) not considered and (b) considered.

CONCLUSION

The results from this study indicate that percent reduction due to creep damage is about the same in magnitude regardless of whether differences in weld regions are considered or not. However, it is also clear that the magnetic changes due to differences in weld regions have to first be calibrated before a quantitative creep damage measurement can be done.

In practice, the creep damage in power plant steam pipes is known to be greatest in the middle of the pipe length and is very minimal at the ends of the steam pipes near the butt welds. [11] The magnetic properties due to the seam weld only can thus be calibrated by first doing measurements at the pipe ends and then by comparing those measurements to the measurements done along the rest of the pipe length.

ACKNOWLEDGMENTS

This work was supported under EPRI Contract WO5295-01.

REFERENCES

1. J.L. Landrum and S.M. Walker, "Guidelines for the evaluation of seam-welded high energy piping", *Final Report to Electric Power Research Institute TR-104631*, 1995 (unpublished)
2. N.L. Loh, Brit. J. NDT 31, 437 (1989)
3. Z.J. Chen, M.R. Govindaraju, D.C. Jiles, S.B. Biner, and M.J. Sablik, IEEE Trans. Magn. 30, 4596 (1994)
4. M.J. Sablik and D.C. Jiles, in *Nondestructive Evaluation of Utilities and Pipelines*, SPIE Volume 2947 (SPIE, Bellingham, WA, 1996), p. 166
5. M.J. Sablik, S. Rubin, D.C. Jiles, D. Kaminski, and Y. Bi, IEEE Trans. Magn. 32, 4290 (1996)
6. D.C. Jiles and D.L. Atherton, J. Magn. Magn. Mater. 6, 48 (1986)
7. M.J. Sablik and D.C. Jiles, IEEE Trans. Magn. 29, 2113 (1993)
8. M.J. Sablik, G.L. Burkhardt, H. Kwun, and D.C. Jiles, J. Appl. Phys. 63, 3930 (1988)
9. S.M. Thompson, P.J. Allen, and B.K. Tanner, IEEE Trans. Magn. 26, 1984 (1990)
10. D.C. Jiles, J.B. Thoelke, and M.K. Devine, IEEE Trans. Magn. 28, 27 (1992)
11. R. Tilley, Electric Power Research Institute, private communication